# Manganese-Porphyrin-Catalyzed C-H Fluorination: Hydrocarbons, But Not Drugs?

Vyshnavi Vennelakanti[1,2,3*], Usa Reilly[4], Anton V. Sinitskiy[3**]

[1]*Department of Chemical Engineering, Massachusetts Institute of Technology, Cambridge, MA 02139, USA*

[2]*Department of Chemistry, Massachusetts Institute of Technology, Cambridge, MA 02139, USA*

[3]*Pfizer Worldwide Research and Development, Cambridge, MA 02139, USA*

[4]*Pfizer Worldwide Research and Development, Groton, CT 06340, USA*

* This project was carried out during an internship of V.V. at Pfizer.

** Email: anton.sinitskiy@pfizer.com

**Abstract**

Transformation of C-H to C-F bonds in organic compounds can be used in drug design to easily diversify molecular series under exploration. A particularly attractive fluorination reaction is the recently discovered aliphatic C-H bonds fluorination catalyzed by manganese(Mn)-containing porphyrins, which proceeds under mild conditions and with high yields[1-2]. However, this fluorination technique has been applied so far only to a narrow range of carbon rich organic substrates. In this preliminary study, based on quantum chemical modeling of several key stages in the presumed mechanism of this reaction, we put forward a hypothesis to explain difficulties of extending the Mn-porphyrin-catalyzed fluorination to nitrogen rich drug-like molecules, namely, a significant growth of the height of the activation barrier for drug-like substrates. Specifically, we demonstrate that reaction energies are comparable for various substrates, including those for which Mn-porphyrin-catalyzed fluorination occurs and those for which it does not occur, and hence, thermodynamic factors are unlikely to control the observed differences in the reactivity. Next, we carry out a first-pass modeling of fluorination reaction paths for two substrates, cyclohexane versus piperidine, as a representative of the type of nitrogen rich compound that can and cannot be fluorinated under recommended conditions, and found a significant difference in activation energies (~7 kcal/mol vs ~40 kcal/mol), which might point at the reason for the difference in the reactivity. Further computational modeling is required to reveal the limitations of the Mn-porphyrin-catalyzed fluorination, and, if possible, possible ways to overcome such limitations.

## 1. Introduction

Selective C–H functionalization plays an important role[3] in the synthesis of bioactive natural products[4-14], drug metabolism[15-16], pharmaceutical industry[17-23], DNA repair[24-27], and transcription[28-30]. C–H bonds can be functionalized in various ways, including but not limited to cyanation[31-38], oxidation[39], hydroxylation[40], epoxidation[41-42], and halogenation[43-45]. Activation of unreactive C–H bonds typically requires harsh conditions[46] due to the high C–H bond dissociation energy[15] and its inert nature[47]. While C–H halogenation is widely used, C–H fluorination is a difficult process, oftentimes requiring special safety equipment and highly reactive reagents[48-54]. Despite the difficulties, several studies were carried out to understand C–H fluorination since it might play a crucial role in drug development[23, 55-59].

Transition metal catalysts are widely used for direct and selective C–H functionalization[60]. While late transition metals like palladium have been frequently used in experimental studies in the past[60-67], recent studies are shifting towards the use of catalysts containing manganese, iron, cobalt, nickel[68], etc. as they show comparable or even better reactivity than the late transition metal catalysts[60, 69-71]. Of the mid-row 3*d* metal catalysts, manganese catalysts for C–H fluorination look particularly attractive due to the non-toxicity of manganese, its relatively low cost, and environment friendly characteristics[60, 67, 72-74]. Manganese enzymes[75] found in nature can activate C–H bonds with high dissociation energy, which led to development of bioinspired molecular catalysts[60].

Several experimental studies and few computational studies considered Mn-porphyrin catalysts and Mn-salen catalysts to carry out C–H halogenation, in particular, C–H fluorination[1-2, 76-77]. Manganese-catalyzed oxidative benzylic C–H fluorination was shown to be accomplished with better yields using Mn-salen catalysts[2]. Mn-porphyrin complexes were found to catalyze selective aliphatic C–H bond halogenations with remarkable yields for a certain range of organic substrates[1, 76]. However, our attempts to fluorinate drug-like molecules (e.g., containing heterocycles with N or O atoms) under the same experimental conditions were excluded. The reasons for this inapplicability of the published procedures of synthesis to drug-like molecules, as far as we know, are unclear.

Manganese exists in different oxidation states in the intermediates formed during a catalytic cycle[1-2, 76, 78-81]. The presence of unpaired *d* electrons indicates a possibility of multiple spin states for each intermediate. While most experimental studies agree upon the coarse details of the mechanism, these studies disagree in terms of the oxidation state of manganese and the charge of the intermediates[1-2, 76, 78-81]. Additionally, the literature on identifying the ground spin states of each of these intermediates in the catalytic cycle is sparse. A few computational studies considered some but not all the possible spin states for these intermediates[82]. The role of ground spin state is crucial because the reactivity of transition metal catalysts is known to be strongly spin-state dependent[83-93] with several molecular catalysts as well as enzymes preferring high-spin (HS) intermediates during the reaction[94-102].

While prior studies demonstrate successful fluorination of some substrates, typically without heteroatoms[76-81], pharmacologically-active drugs often involve the presence of fluorine in heterocycle rings, steroids (and their derivatives), etc., including N and/or O heteroatoms[103]. In this study, we first aim to understand the ground spin state of the Mn-porphyrin intermediates as predicted by hybrid density functional theory (DFT) and its sensitivity to the functional. We then compute reaction energies along the catalytic cycle for substrates used in prior experimental studies[76] to estimate a possible role of thermodynamic factors in the control of reactivity and regioselectivity of Mn-porphyrin-catalyzed fluorination. Lastly, we obtain potential energy curves along the reaction coordinate for C–H fluorination, for the simplest cases of cyclohexane and piperidine (representatives of active and non-active substrates, respectively, for Mn-porphyrin-catalyzed fluorination) to understand why fluorination of drug-like compounds with heteroatoms does not occur as simply as fluorination of hydrocarbons.

## 2. Reaction Mechanism

We accept in this work the reaction mechanism suggested in prior studies[1-2, 78-79] for aliphatic C-H fluorination with Mn complexes. In the resting state (**1**), the catalyst consists of Mn(III) coordinated to tetramesitylporphyrin (TMP) in the equatorial plane and fluoride in an axial position, with the other axial position being vacant (Figure 1). Oxidation of this resting state intermediate results in a highly reactive oxomanganese species (**2**), Mn(V)=O(TMP)F (Figure 1). This reactive Mn(V)-oxo intermediate abstracts a hydrogen atom from the substrate to form Mn(IV)-hydroxo intermediate (**3**), Mn(IV)(OH)(TMP)F, and a radical located on a carbon atom of the substrate (Figure 1). The next step involves the formation of a difluoro intermediate (**4**), Mn(IV)(TMP)$F_2$, by replacing OH with F in the catalyst in the reaction with AgF (Figure 1). The fluoride in the axial position of the Mn(IV)(TMP)$F_2$ intermediate then combines with the substrate radical to form the fluorinated product. This step is believed to be rate-limiting in the mechanism of the fluorination reaction. After this stage, the catalyst returns to its resting state (Figure 1). Manganese exhibits different oxidation states in the intermediates formed during the catalytic cycle which gives rise to the possibility of multiple spin states for each intermediate. In this work, we modeled all the intermediates in all possible spin states to identify the ground spin state for each intermediate.

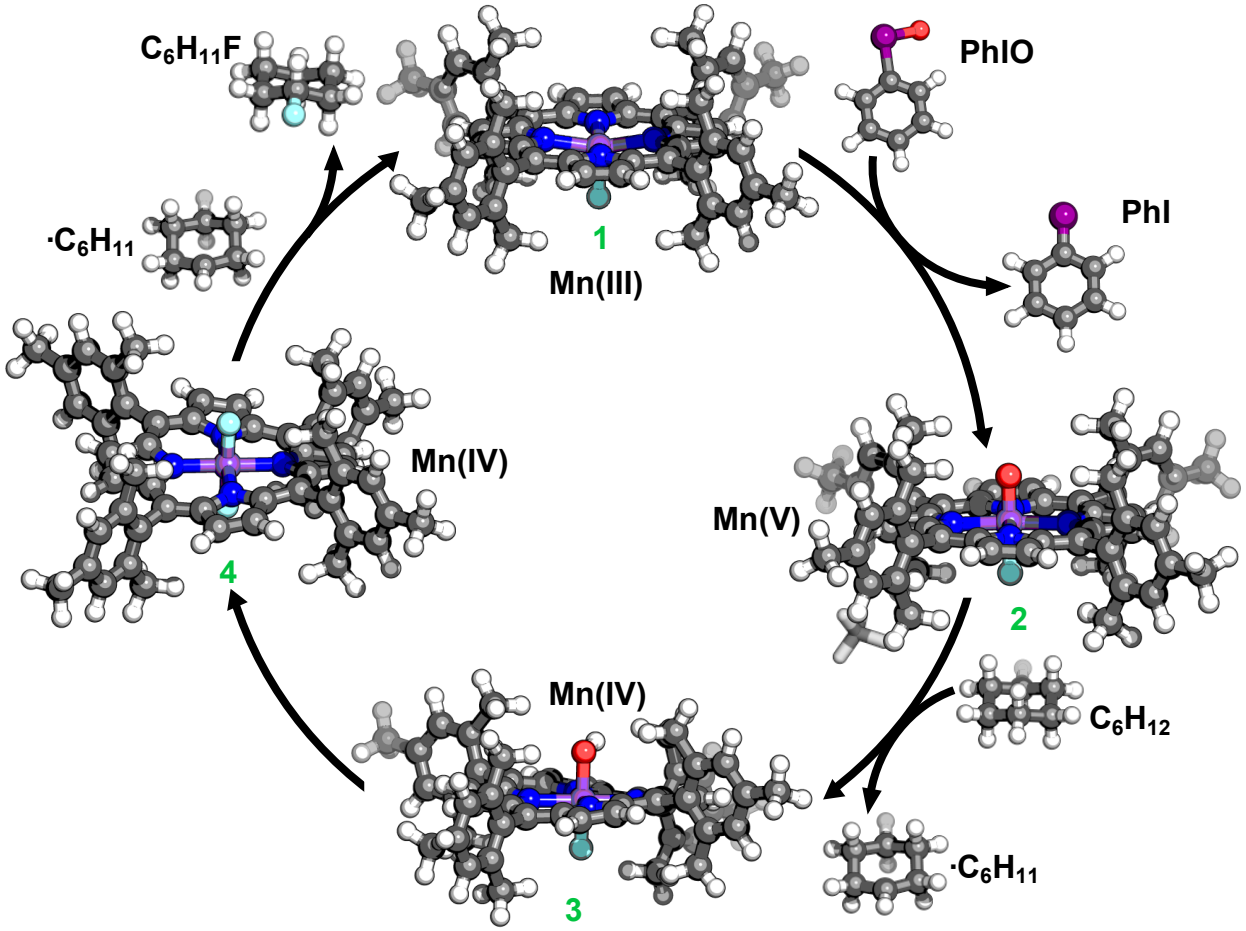


**Figure 1.** Proposed[1-2, 78-79] reaction mechanism for C-H fluorination with Mn(TMP)F catalyst (clockwise, top to bottom): resting state intermediate, Mn(III)(TMP)F (**1**), oxomanganese intermediate, Mn(V)=O(TMP)F (**2**), hydroxo bound to metal, Mn(IV)(OH)(TMP)F (**3**), and difluoro intermediate, Mn(IV)(TMP)$F_2$ (**4**). As an example, the substrate cyclohexane ($C_6H_{12}$), the substrate radical cyclohexyl radical ($\cdot C_6H_{11}$), and fluorinated product, fluorocyclohexane ($C_6H_{11}F$) are also shown. Ball and stick structures are colored by element as: hydrogen in white, carbon in gray, nitrogen in blue, oxygen in red, fluorine in cyan, manganese in purple, and iodine in dark purple.

## 3. Computational Details

Initial structures for substrates, intermediate radicals, fluorinated products, and the Mn(TMP) catalyst used in prior experimental studies[1] were built in Avogadro v1.2.0[104]. These structures were then force-field optimized in Avogadro using UFF force field[105]. Besides isolated complexes, geometries were also built for intermediates formed during the catalytic cycle[1] (see Section 2). Unconstrained geometry optimizations were carried out with TeraChem[106] using hybrid B3LYP[107-109] density functional theory (DFT) where semi-empirical D3[110] dispersion with Becke-Johnson[111] damping was incorporated. The multibasis feature of TeraChem was employed, with the LANL2DZ[112-113] effective core potential (ECP) used for Mn and Cl, and 6-31G*[114] basis set for all other atoms. All optimization calculations were carried out in Cartesian coordinates using L-BFGS algorithm implemented in DL-FIND[115] with the default thresholds of 4.5 x $10^{-4}$ hartree per bohr for the maximum gradient and 1 x $10^{-6}$ hartree for self-consistent field (SCF) convergence. Level-shifting[116] values of 0.25 hartree were applied for both occupied and virtual orbitals for open-shell calculations which were carried out in a spin-unrestricted formalism. Closed-shell singlet calculations were carried out in a spin-restricted formalism.

All calculations were performed in the presence of an implicit solvent with a dielectric constant, ε, of 30.4 which was computed as a weighted average of dielectric constants of one part of dichloromethane (ε = 8.9) and three parts of acetonitrile (ε = 37.5), consistent with prior experimental studies[1]. A conductor-like polarizable continuum implicit solvent model[117-118] implemented in TeraChem[119] was employed in these calculations. The solute cavity for non-metals was constructed with default parameters of 1.2 x Bondi's van der Waals radii[120] available in TeraChem. Additionally, for Mn, we adopted the procedure employed in prior

studies[121] where the standard van der Waals radius[122] of Mn was scaled by 1.2.

Optimization calculations of the Mn(TMP) catalyst were carried out in all possible spin states for each intermediate formed during the catalyst cycle. Specifically, the resting state intermediate, Mn(III)(TMP)F with a $d^4$ electronic configuration for Mn, was studied in three spin states: high-spin (HS) quintet, intermediate-spin (IS) triplet, and low-spin (LS) singlet. The oxomanganese intermediate, Mn(V)=O(TMP)F with a $d^2$ electronic configuration for Mn, was studied in two possible spin states: IS triplet and LS singlet. The metal-hydroxo and difluoro intermediates, Mn(IV)(OH)(TMP)F and Mn(IV)(TMP)$F_2$, both with a $d^3$ electronic configuration for Mn were studied in the two possible spin states: IS quartet and LS doublet. All calculations of the catalyst intermediates were carried out at the B3LYP-D3/LACVP* level of theory where we varied the amount of Hartree-Fock exchange ($a_{HF}$) incorporated in the density functional from 0.00 to 0.30 in increments of 0.10, while holding the LDA/GGA exchange ratio fixed, in order to study the sensitivity of the predicted ground state to the density functional used[123-124]. All the calculations were found to be free of significant spin contamination, evaluated as the difference between the computed expectation of $\hat{S}^2$ operator and the expected value, i.e., $S(S+1)$.

One dimensional (1D) potential energy curves (PECs) to identify energetic changes during fluorination of the substrate radical and the corresponding putative transition state were also carried out in TeraChem. The structures along the reaction coordinate, which was chosen to be the distance between the carbon radical of the substrate and the fluoride of catalyst (C···F), were generated by molSimplify[125], which uses OpenBabel[126-127] as a backend, in intervals of 1.50 Å. Constrained optimizations in the presence of an implicit solvent (ε = 30.4) at B3LYP-D3/LACVP* level of theory were carried out for these structures where the heavy atoms of the catalyst and the carbon radical of the substrate were constrained, while the rest of the system was allowed to relax.

## 4. Results and Discussion

### 4.a. Ground spin states of intermediates

We compute energies of intermediates using B3LYP hybrid density functional theory to predict the ground spin state of various intermediates along the catalytic cycle. We then vary the amount of Hartree-Fock exchange ($a_{HF}$) in the functional to understand the dependence of energetics on the functional. For each intermediate, we compute the difference of energies between various spin states, and thereby identify the ground spin state.

For the resting state intermediate (**1**), we find that high-spin (HS) quintet is the preferred ground-state irrespective of the amount of Hartree-Fock exchange in the functional (Table 1). However, closer inspection reveals that the difference in energetics between the HS and intermediate-spin (IS) states is high at higher $a_{HF}$, while at $a_{HF}$ = 0.00, both HS and IS states are comparable in energy (differ by ca. 1 kcal/mol, Table 1).

For the manganese-oxo intermediate (**2**), we could not identify the ground spin state at lower $a_{HF}$ values due to convergence issues. At higher $a_{HF}$ values, we see that IS triplet state is preferred (Table 1). However, we see that the difference in energetics becomes more and more negative with increasing $a_{HF}$, i.e., the difference in energies ranges from ca. -7 kcal/mol at $a_{HF}$ = 0.20 to -23 kcal/mol at $a_{HF}$ = 0.30. This may indicate that at lower $a_{HF}$ values (0.00 and 0.10), the preferred ground state could be the low-spin (LS) singlet state (Table 1). For both the resting state intermediate and the manganese-oxo intermediate, we find an increasing preference of higher spin states at higher $a_{HF}$ values (Table 1).

In contrast to these observations, for manganese-hydroxo and manganese-difluoro intermediates, we find a strong preference for lower spin states with increasing $a_{HF}$ in the functional (Table 1).

Overall, we observe that the predicted ground state is strongly dependent on the amount of Hartree-Fock exchange in a functional. One would hardly be able to identify the ground spin states of various intermediates formed along the catalytic cycle only with DFT. Calculations with more accurate wavefunction theory methods might identify the ground spin state of these intermediates with more certainty, but such computations would also be much more – if not prohibitively – expensive for such large molecular systems. Also, relatively small energy gaps between different spin states predicted with some versions of the density functional, comparable to the scale of thermal fluctuations (~$kT$), might imply that different spin states may coexist at equilibrium, and that ratio of different spin forms may be highly sensitive to various conditions, such as temperature, as well as modifications of the structure of the ligand. To the best of our knowledge, no experimental studies have addressed these issues of relative stability and possible coexistence of various spin forms of the Mn-porphyrin catalytic complexes.

Given the preference of higher spin state of the Mn(V)-oxo intermediate from other literature studies[98, 101-102], we move forward in this work assuming a mechanism where the higher-spin states are the preferred ground states for all the intermediates, i.e., HS quintet and IS triplet for the resting state intermediate and the manganese-oxo intermediate, respectively, and IS quartet for manganese-hydroxo and manganese-difluoro intermediates.

**Table 1.** Difference in energies between various spin states of the four intermediates along the catalytic cycle at various Hartree-Fock exchange fractions $a_{HF}$. $\Delta E_{H\text{-}I}$, $\Delta E_{H\text{-}L}$, and $\Delta E_{I\text{-}L}$ correspond to differences in energies between HS and IS, HS and LS, and IS and LS states, respectively. Calculations could not be converged for intermediates indicated by **.

| **$a_{HF}$ = 0.00** | | | | |
|---|---|---|---|---|
| **Intermediate** | **$\Delta E_{H\text{-}I}$ (kcal/mol)** | **$\Delta E_{H\text{-}L}$ (kcal/mol)** | **$\Delta E_{I\text{-}L}$ (kcal/mol)** | **Ground state** |
| Mn(III)(TMP)F | -1.01 | -28.34 | -27.33 | HS quintet |
| Mn(V)=O(TMP)F** | --- | --- | --- | --- |
| Mn(IV)-OH(TMP)F | --- | --- | -12.29 | IS quartet |
| Mn(IV)-OH(TMP)$F_2$ | --- | --- | -11.27 | IS quartet |
| **$a_{HF}$ = 0.10** | | | | |
| **Intermediate** | **$\Delta E_{H\text{-}I}$ (kcal/mol)** | **$\Delta E_{H\text{-}L}$ (kcal/mol)** | **$\Delta E_{I\text{-}L}$ (kcal/mol)** | **Ground state** |
| Mn(III)(TMP)F | -4.63 | -35.64 | -31.01 | HS quintet |
| Mn(V)=O(TMP)F** | --- | --- | --- | --- |
| Mn(IV)-OH(TMP)F | --- | --- | -10.88 | IS quartet |
| Mn(IV)-OH(TMP)$F_2$ | --- | --- | -7.55 | IS quartet |
| **$a_{HF}$ = 0.20** | | | | |
| **Intermediate** | **$\Delta E_{H\text{-}I}$ (kcal/mol)** | **$\Delta E_{H\text{-}L}$ (kcal/mol)** | **$\Delta E_{I\text{-}L}$ (kcal/mol)** | **Ground state** |
| Mn(III)(TMP)F | -8.32 | -41.77 | -33.55 | HS quintet |
| Mn(V)=O(TMP)F | --- | --- | -6.82 | IS triplet |
| Mn(IV)-OH(TMP)F | --- | --- | -6.97 | IS quartet |
| Mn(IV)-OH(TMP)$F_2$ | --- | --- | -2.71 | IS quartet |
| **$a_{HF}$ = 0.30** | | | | |
| **Intermediate** | **$\Delta E_{H\text{-}I}$ (kcal/mol)** | **$\Delta E_{H\text{-}L}$ (kcal/mol)** | **$\Delta E_{I\text{-}L}$ (kcal/mol)** | **Ground state** |
| Mn(III)(TMP)F | -12.01 | -47.30 | -35.30 | HS quintet |
| Mn(V)=O(TMP)F | --- | --- | -22.78 | IS triplet |
| Mn(IV)-OH(TMP)F | --- | --- | 0.68 | LS doublet |
| Mn(IV)-OH(TMP)$F_2$ | --- | --- | 2.22 | LS doublet |

### 4.b. Reaction energies along the catalytic cycle

Next, we computed reaction energies of a set of substrates studied in prior experimental work (including diastereomers where applicable),[76] supplemented with piperidine. Hydrogen atom transfer (HAT) reaction energy, radical rebound energy, and the fluorinated product release energy were calculated (Figure 2, Table 2). We observe that for almost all the substrates, the HAT energies are comparable (Figure 2, Table 2). For the substrates 1, 2, and 3, which are cyclohexane, cycloheptane, and cyclooctane, the HAT energy becomes slightly more exothermic in moving from the six-membered ring to the eight-membered ring (Figure 2, Table 2). Comparison to rebound energies reveals that HAT energies are ten times less exothermic than rebound energies (Figure 2, Table 2). However, for all substrates, HAT energies are more favorable compared to release energies which are strongly endothermic (Figure 2, Table 2).

Across almost all the substrates, rebound energies are also comparable, as well as release energies (Figure 2, Table 2). Closer examination of rebound energies for cyclohexane and piperidine, which is obtained by replacing a carbon atom of cyclohexane with a nitrogen heteroatom, reveals that rebound energy is slightly more favorable for cyclohexane compared to piperidine (Figure 2, Table 2). A similar comparison of release energies shows that release of fluorinated cyclohexane is slightly more favorable than fluorinated piperidine (Figure 2, Table 2). Therefore, the reaction energies are comparable across different substrates, both capable and incapable of Mn-porphyrin-catalyzed fluorination, and cannot explain this difference in the reactivity.

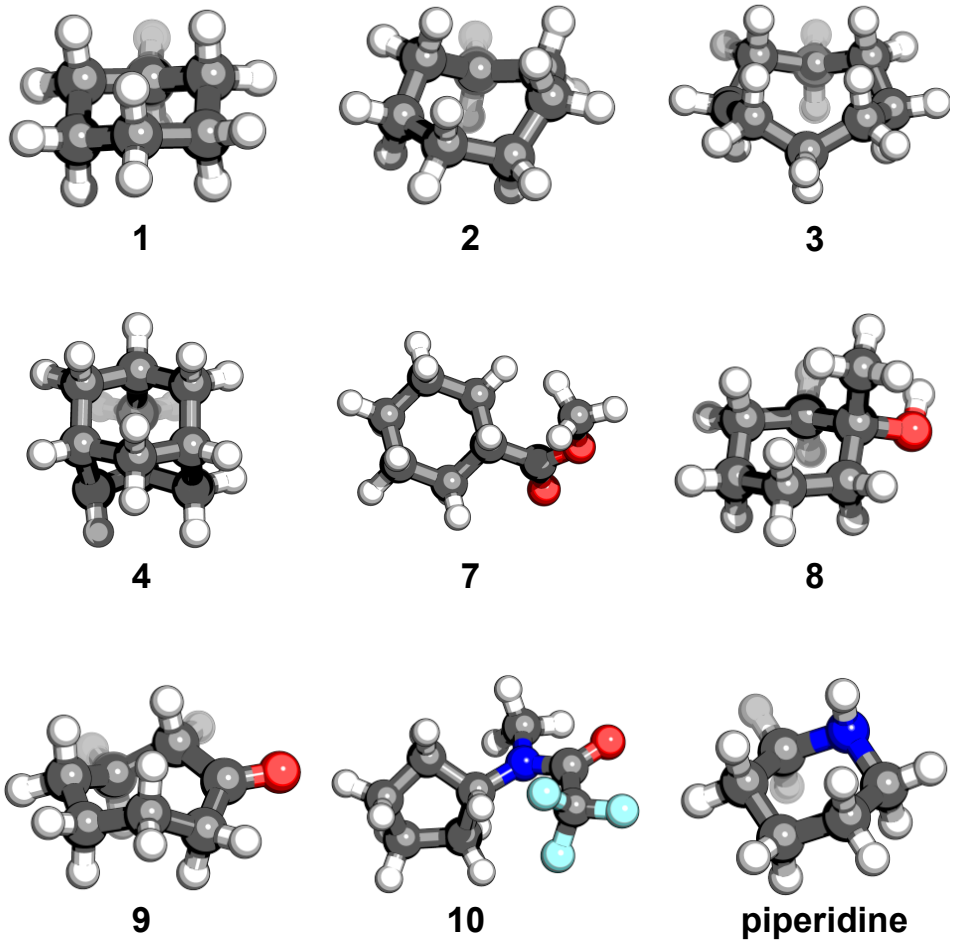


**Figure 2.** Substrates for Mn-porphyrin-catalyzed fluorination from prior experimental work (1-10) and piperidne. Ball and stick structures are colored by element as: hydrogen in white, carbon in gray, nitrogen in blue, oxygen in red, and fluorine in cyan.

**Table 2.** Various reaction energies, namely, hydrogen atom transfer (HAT) energy (column 2), radical rebound energy (column 3), and product release energy (column 4) in kcal/mol for substrates studied in prior experimental work[76] and piperidine. 'a' and 'b' correspond to diastereomers of the corresponding substrate. HAT energy is not available for piperidine.

| Substrates | HAT energy (kcal/mol) | Rebound energy (kcal/mol) | Release energy (kcal/mol) |
|---|---|---|---|
| 1 | -5.14 | -57.26 | 17.14 |
| 2 | -8.72 | -57.17 | 20.61 |
| 3 | -10.30 | -57.01 | 21.17 |
| 4a | -5.58 | -67.05 | 23.62 |
| 4b | -3.98 | -64.83 | 22.82 |
| 7a | -5.23 | -64.39 | 24.96 |
| 7b | -5.21 | -67.14 | 27.23 |
| 8a | -5.65 | -58.01 | 19.13 |
| 8b | -5.23 | -59.34 | 19.25 |
| 9a | -6.63 | -58.11 | 20.06 |
| 9b | -7.54 | -56.61 | 20.72 |
| 10a | -7.64 | -54.37 | 19.26 |
| 10b | -8.29 | -54.47 | 19.73 |
| piperidine | --- | -54.94 | 20.06 |

### 4.c. Potential energy curves for C-H fluorination

In our search for reasons explaining the difference between fluorination of hydrocarbons and drug-like molecules, we hypothesized that they may stem from the kinetic control of this reactions. Based on this hypothesis, we obtain 1D potential energy scans across the fluorination reaction coordinate (Figure 3). We observe that for cyclohexane, the fluorination reaction barrier is ca. 7 kcal/mol and the C-F distance in the putative transition state structure is 2.50 Å (Figure 3). However, for piperidine, we observe that the putative transition state occurs at a shorter C-F distance of 2.35 Å and with almost six times higher energy barrier than that of cyclohexane, ca. 40 kcal/mol (Figure 3), which greatly exceeds the range of thermal fluctuations (~$kT$). We see that while the rebound and release reaction energies are comparable and slightly more favorable for cyclohexane, the reaction barrier for fluorination clearly suggests that fluorination of cyclohexane is strongly preferred whereas the fluorination of piperidine is prohibited (Figure 3). The higher energy barrier could be a result of stabilization of the radical through the lone pair of nitrogen heteroatom. It could also be possible that fluorine forms a more stable complex with this substrate. Further computational studies are necessary to understand why the energy barrier for fluorination of piperidine – and, presumably, drug-like molecules – is so high.

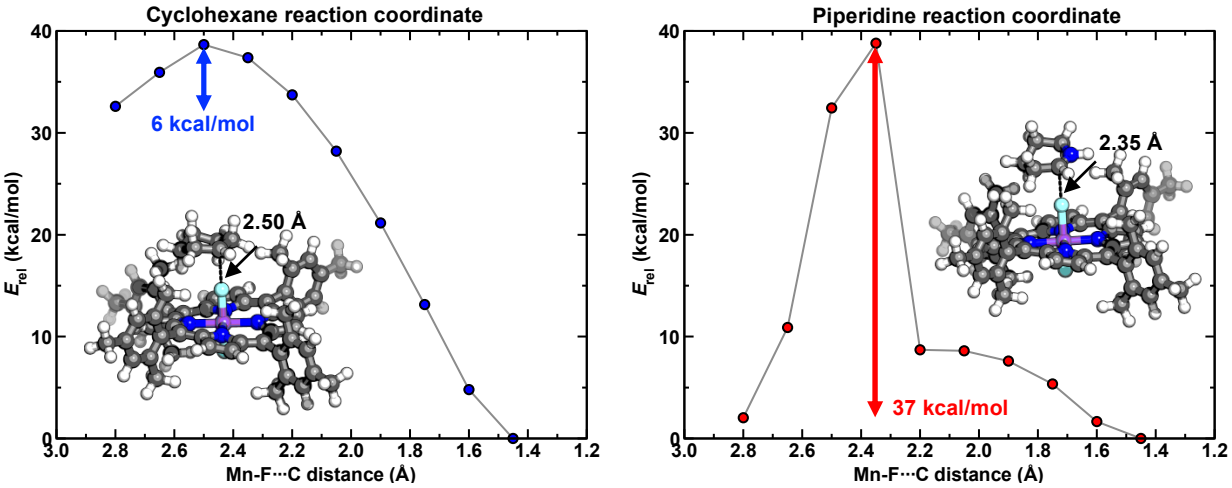


**Figure 3.** 1D potential energy scans for piperidine and cyclohexane. The relative energetics ($E_{rel}$) in kcal/mol are shown as a function of Mn-F···C distance (in Å). Besides the depicted degree of freedom, positions of the heavy atoms of the catalyst and the carbon radical of the substrate were constrained in the interests of computational efficiency, while the other degrees of freedom in the system was allowed to relax. Ball and stick structures for the putative transition states are colored by element as: hydrogen in white, carbon in gray, nitrogen in blue, oxygen in red, fluorine in cyan, and manganese in purple. C···F distance is indicated in the insets.

### 5. Conclusions

Modeling transformation of C-H bonds to C-F bonds is of high practical importance because such reactions may extend our abilities to optimize potency; absorption, distribution, metabolism, excretion, and toxicity (ADMET) and physico-chemical properties of drug candidates. Prediction of the rate and stereoselectivity of fluorination of various substrates in such reactions under various conditions could significantly speed up rational drug design and manufacturing optimization. Unfortunately, the current understanding of such reactions leave multiple questions unanswered, including the reasons why the recently discovered and very promising aliphatic C-H bonds fluorination catalyzed by Mn-containing porphyrins may be not applicable to drug-like molecules. In this work, we attempt to start filling out this gap in the knowledge.

In this study, firstly, we looked at the ground spin states of various intermediates observed along the C-H fluorination catalytic cycle. We observed that the energies of various spin states are close to each other (differences comparable to $kT$), and the identification of the ground state is highly sensitive to the used density functional. We hypothesize that the Mn complex may enter the rate-limiting step of the catalytic cycle most likely in an intermediate-spin quartet state, though the low-spin doublet state may also be reachable in terms of energy. More accurate and much more expensive wavefunction theory methods might help further clarify the ground state of these intermediates with more certainty. On the other hand, relatively small differences in the predicted energies of various spin states may imply that the ground states are sensitive to experimental conditions under which fluorination is performed, and transitions between different spin states might be a real phenomenon rather than a computational artifact. If so, this observation may suggest an additional potential direction to

control the regioselectivity and yield of the reaction via factors that affect the spin states, e.g., by modifications of the peripheral parts of the porphyrin ligand, which would fine tune the strength of the ligand field. Secondly, we looked at the reaction energies for various substrates and found that the reaction energies of active and inactive substrates are mostly comparable, indicating that thermodynamic factors may not play the central role in determining whether a certain substrate molecule can undergo catalyzed fluorination. Thirdly, based on these results, we hypothesized that the determining factor might be the reaction barrier and the properties of the corresponding transition state. For a preliminary estimation of plausibility of such an explanation, we carried out 1D potential energy scans for reaction pathways for piperdine and cyclohexane, and found that the energy barrier for fluorination of piperidine is almost six times higher than that of cyclohexane, and significantly exceeds the energies reachable by thermal fluctuations, in agreement with the assignment of these two substrates to non-reactive and reactive classes, respectively. We speculate that the high energy barrier in case of piperidine could be due to the formation of a more stable substrate system due to the lone pair of nitrogen stabilizing the carbon radical or the formation of a more stable complex with fluorine. This interpretation, however, requires further computational investigation. While we modeled Mn-porphyrin complexes in this work, some of our results may be relevant for understanding other fluorination reactions, for example, benzylic C–H fluorination using Mn-salen catalysts.

Limitations of this study include the use of inexpensive (and therefore, not the most accurate) DFT functionals, modeling a limited set of substrates (especially in the third part of the work), inexhaustive sampling of the configuration space in transition state modeling, and, most importantly, the absence of experimental verification of the key conclusions. However, we believe that given the current state of the knowledge on Mn-porphyrin-catalyzed fluorination, our paper will contribute to the progress in understanding such reactions by identifying promising directions of further research.

We expect that future work on computational modeling of Mn-porphyrin-catalyzed fluorination, based on intelligent reconstruction of transition states for the limiting stage of the catalytic cycle, and quantum chemical simulations of properties of these transition states, will be able to guide substrate-specific optimization of the reaction conditions, including the catalyst optimization, and predict regioselectivity of functionalization of a given substrate under given conditions. The *ab initio* character of such models would allow for better extrapolations to new substrates. A combination of computational modeling and experimental studies is also highly desirable. Overall, Mn-porphyrin-catalyzed fluorination of organic substrates is a promising, but still problematic technique, and its improvements may be guided by computational modeling of transitions states in these reactions.

## Conflicts of Interests

The authors declare no competing financial interest.


## Acknowledgements

We would like to thank Dr. Brajesh K. Rai for invaluable discussion and a general support to this project.


## References


1.Liu, W.; Huang, X. Y.; Cheng, M. J.; Nielsen, R. J.; Goddard, W. A.; Groves, J. T., Oxidative Aliphatic C-H Fluorination with Fluoride Ion Catalyzed by a Manganese Porphyrin. *Science* **2012,** *337* (6100), 1322-1325.

2.Liu, W.; Groves, J. T., Manganese-Catalyzed Oxidative Benzylic C-H Fluorination by Fluoride Ions. *Angew Chem Int Edit* **2013,** *52* (23), 6024-6027.

3.Gandeepan, P.; Muller, T.; Zell, D.; Cera, G.; Warratz, S.; Ackermann, L., 3d Transition Metals for C-H Activation. *Chem Rev* **2019,** *119* (4), 2192-2452.

4.Karimov, R. R.; Hartwig, J. F., Transition-Metal-Catalyzed Selective Functionalization of C(sp(3))-H Bonds in Natural Products. *Angew Chem Int Edit* **2018,** *57* (16), 4234-4241.

5.Brady, P. B.; Bhat, V., Recent Applications of Rh- and Pd-Catalyzed C(sp(3))-H Functionalization in Natural Product Total Synthesis. *Eur J Org Chem* **2017,** *2017* (35), 5179-5190.

6.Sinha, S. K.; Zanoni, G.; Maiti, D., Natural Product Synthesis by C-H Activation. *Asian J Org Chem* **2018,** *7* (7), 1178-1192.

7.Qiu, Y. Y.; Gao, S. H., Trends in applying C-H oxidation to the total synthesis of natural products. *Natural Product Reports* **2016,** *33* (4), 562-581.

8.Yamaguchi, J.; Yamaguchi, A. D.; Itami, K., C-H Bond Functionalization: Emerging Synthetic Tools for Natural Products and Pharmaceuticals. *Angew Chem Int Edit* **2012,** *51* (36), 8960-9009.

9.Rossi, R.; Lessi, M.; Manzini, C.; Marianetti, G.; Bellina, F., Direct (Hetero) arylation Reactions of (Hetero) arenes as Tools for the Step-and Atom-Economical Synthesis of Biologically Active Unnatural Compounds Including Pharmaceutical Targets. *Synthesis-Stuttgart* **2016,** *48* (22), 3821-3862.

10.Chen, D. Y. K.; Youn, S. W., C-H Activation: A Complementary Tool in the Total Synthesis of Complex Natural Products. *Chem-Eur J* **2012,** *18* (31), 9452-9474.

11.Cochrane, R. V. K.; Vederas, J. C., Highly Selective but Multifunctional Oxygenases in Secondary Metabolism. *Accounts Chem Res* **2014,** *47* (10), 3148-3161.

12.Lewis, J. C.; Coelho, P. S.; Arnold, F. H., Enzymatic functionalization of carbon-hydrogen bonds. *Chem Soc Rev* **2011,** *40* (4), 2003-2021.

13.Krebs, C.; Fujimori, D. G.; Walsh, C. T.; Bollinger Jr., J. M., Non-Heme Fe(IV)-Oxo Intermediates. *Accounts Chem Res* **2007,** *40* (7), 484-492.

14.Walsh, C. T., The Chemical Versatility of Natural-Product Assembly Lines. *Accounts Chem Res* **2008,** *41* (1), 4-10.

15.Groves, J. T., ENZYMATIC C-H BOND ACTIVATION Using push to get pull. *Nat Chem* **2014,** *6* (2), 89-91.
16.de Montellano, P. R. O., Hydrocarbon Hydroxylation by Cytochrome P450 Enzymes. *Chemical Reviews* **2010,** *110* (2), 932-948.
17.Nakama, Y.; Yoshida, O.; Yoda, M.; Araki, K.; Sawada, Y.; Nakamura, J.; Xu, S.; Miura, K.; Maki, H.; Arimoto, H., Discovery of a novel series of semisynthetic vancomycin derivatives effective against vancomycin-resistant bacteria. *Journal of Medicinal Chemistry* **2010,** *53*, 2528-2533.
18.Seki, M., A New Catalytic System for Ru-Catalyzed C-H Arylation Reactions and Its Application in the Practical Syntheses of Pharmaceutical Agents. *Org Process Res Dev* **2016,** *20* (5), 867-877.
19.Ackermann, L., Robust Ruthenium(II)-Catalyzed C-H Arylations: Carboxylate Assistance for the Efficient Synthesis of Angiotensin-II-Receptor Blockers. *Org Process Res Dev* **2015,** *19* (1), 260-269.
20.Baldwin, J. E.; Bradley, M., Isopenicillin-N Synthase - Mechanistic Studies. *Chem Rev* **1990,** *90* (7), 1079-1088.
21.Choroba, O. W.; Williams, D. H.; Spencer, J. B., Biosynthesis of the vancomycin group of antibiotics: Involvement of an unusual dioxygenase in the pathway to (S)-4-hydroxyphenylglycine. *J Am Chem Soc* **2000,** *122* (22), 5389-5390.
22.Muller, K.; Faeh, C.; Diederich, F., Fluorine in pharmaceuticals: Looking beyond intuition. *Science* **2007,** *317* (5846), 1881-1886.
23.Gillis, E. P.; Eastman, K. J.; Hill, M. D.; Donnelly, D. J.; Meanwell, N. A., Applications of Fluorine in Medicinal Chemistry. *Journal of Medicinal Chemistry* **2015,** *58* (21), 8315-8359.
24.Trewick, S. C.; Henshaw, T. F.; Hausinger, R. P.; Lindahl, T.; Sedgwick, B., Oxidative demethylation by Escherichia coli AlkB directly reverts DNA base damage. *Nature* **2002,** *419* (6903), 174-178.
25.Falnes, P. O.; Johansen, R. F.; Seeberg, E., AlkB-mediated oxidative demethylation reverses DNA damage in Escherichia coli. *Nature* **2002,** *419* (6903), 178-182.
26.Yi, C.; Jia, G.; Hou, G.; Dai, Q.; Zhang, W.; Zheng, G.; Jian, X.; Yang, C.-G.; Cui, Q.; He, C., Iron-Catalysed Oxidation Intermediates Captured in a DNA Repair Dioxygenase. *Nature* **2010,** *468* (7321), 330-333.
27.Duncan, T.; Trewick, S. C.; Koivisto, P.; Bates, P. A.; Lindahl, T.; Sedgwick, B., Reversal of DNA alkylation damage by two human dioxygenases. *Proceedings of the National Academy of Sciences of the United States of America* **2002,** *99* (26), 16660-16665.
28.Cloos, P. A. C.; Christensen, J.; Agger, K.; Maiolica, A.; Rappsilber, J.; Antal, T.; Hansen, K. H.; Helin, K., The putative oncogene GASC1 demethylates tri- and dimethylated lysine 9 on histone H3. *Nature* **2006,** *442* (7100), 307-311.
29.Klose, R. J.; Yamane, K.; Bae, Y.; Zhang, D.; Erdjument-Bromage, H.; Tempst, P.; Wong, J.; Zhang, Y., The transcriptional repressor JHDM3A demethylates trimethyl histone H3 lysine 9 and lysine 36. *Nature* **2006,** *442* (7100), 312-316.
30.Tsukada, Y.-i.; Fang, J.; Erdjument-Bromage, H.; Warren, M. E.; Borchers, C. H.; Tempst, P.; Zhang, Y., Histone demethylation by a family of JmjC domain-containing proteins. *Nature* **2006,** *439* (7078), 811-816.
31.Zhao, C. Y.; Yang, S. W.; Cheng, Y. X.; Qu, R. X.; Huang, X. R.; Liu, H. L., Mechanistic Insight into Pd(II)-Catalyzed Late-Stage Non-directed C(sp(2))-H Cyanation of Toluene Using the Dual Ligands MPAA and Quinoxaline: A Density Functional Theory Investigation. *J Org Chem* **2021,** *86* (15), 10526-10535.
32.Deng, C.; Sun, Y. X.; Ren, Y.; Zhang, W. H., Theoretical studies on Rh(III)-catalyzed regioselective C-H bond cyanation of indole and indoline. *Dalton T* **2019,** *48* (1), 168-175.
33.Su, Z. S.; Hu, C. W.; Shahzad, N.; Kim, C. K., Asymmetric Cyanation of Activated Olefins with Ethyl Cyanoformate Catalyzed by Ti(IV)-Catalyst: A Theoretical Study. *Catalysts* **2020,** *10* (9).
34.Yang, Y.; Buchwald, S. L., Copper-Catalyzed Regioselective ortho C-H Cyanation of Vinylarenes. *Angew Chem Int Edit* **2014,** *53* (33), 8677-8681.
35.Zhou, D. G.; Yang, F.; Yang, X.; Yan, C. X.; Zhou, P. P.; Jing, H. W., Mechanism of selective C-H cyanation of 2-phenylpyridine with benzyl nitrile catalyzed by CuBr: a DFT investigation. *Org Chem Front* **2017,** *4* (3), 377-385.
36.Pal, P.; Mondal, S.; Chatterjee, A.; Saha, R.; Chakrabarty, K.; Das, G. K., Revisited the mechanism of cobalt(III) catalyzed cyanation of arenes and heteroarenes: A DFT study. *Comput Theor Chem* **2021,** *1201*.
37.Detmar, E.; Muller, V.; Zell, D.; Ackermann, L.; Breugst, M., Cobalt-catalyzed C-H cyanations: Insights into the reaction mechanism and the role of London dispersion. *Beilstein J Org Chem* **2018,** *14*, 1537-1545.
38.Zhang, W.; Wang, F.; McCann, S. D.; Wang, D. H.; Chen, P. H.; Stahl, S. S.; Liu, G. S., Enantioselective cyanation of benzylic C-H bonds via copper-catalyzed radical relay. *Science* **2016,** *353* (6303), 1014-1018.
39.Dick, A. R.; Hull, K. L.; Sanford, M. S., A highly selective catalytic method for the oxidative functionalization of C-H bonds. *J Am Chem Soc* **2004,** *126* (8), 2300-2301.
40.Dunham, N. P.; Mitchell, A. J.; Pantoja, J. M. D.; Krebs, C.; Bollinger, J. M.; Boal, A. K., alpha-Amine Desaturation of D-Arginine by the Iron(II)- and 2-(Oxo)glutarate-Dependent L-Arginine 3-Hydroxylase, VioC. *Biochemistry* **2018,** *57* (46), 6479-6488.
41.Pappalardo, A.; Ballistreri, F. P.; Toscano, R. M.; Chiacchio, M. A.; Legnani, L.; Grazioso, G.; Veltri, L.; Sfrazzetto, G. T., Alkene Epoxidations Mediated by Mn-Salen Macrocyclic Catalysts. *Catalysts* **2021,** *11* (4).
42.Espinoza, R. V.; Haatveit, K. C.; Grossman, S. W.; Tan, J. Y.; McGlade, C. A.; Khatri, Y.; Newmister, S. A.; Schmidt, J. J.; Garcia-Borras, M.; Montgomery, J.; Houk, K. N.; Sherman, D. H., Engineering P450 TamI as an Iterative Biocatalyst for Selective Late-Stage C-H Functionalization and Epoxidation of Tirandamycin Antibiotics. *Acs Catalysis* **2021,** *11* (13), 8304-8316.
43.Giri, R.; Chen, X.; Yu, J. Q., Palladium-catalyzed asymmetric iodination of unactivated C-H bonds under mild conditions. *Angew Chem Int Edit* **2005,** *44* (14), 2112-2115.
44.Kalyani, D.; Dick, A. R.; Anani, W. Q.; Sanford, M. S., A simple catalytic method for the regioselective halogenation of arenes. *Org Lett* **2006,** *8* (12), 2523-2526.
45.Kalyani, D.; Dick, A. R.; Anani, W. Q.; Sanford, M. S., Scope and selectivity in palladium-catalyzed directed C-H bond halogenation reactions. *Tetrahedron* **2006,** *62* (49), 11483-11498.

46.Prakash, G. S.; Mathew, T.; Hoole, D.; Esteves, P. M.; Wang, Q.; Rasul, G.; Olah, G. A., N-Halosuccinimide/BF3− H2O, efficient electrophilic halogenating systems for aromatics. *J Am Chem Soc* **2004,** *126* (48), 15770-15776.
47.Altus, K. M.; Love, J. A., The continuum of carbon-hydrogen (C-H) activation mechanisms and terminology. *Commun Chem* **2021,** *4* (1).
48.Yamamoto, K.; Li, J. K.; Garber, J. A. O.; Rolfes, J. D.; Boursalian, G. B.; Borghs, J. C.; Genicot, C.; Jacq, J.; van Gastel, M.; Neese, F.; Ritter, T., Palladium-catalysed electrophilic aromatic C-H fluorination. *Nature* **2018,** *554* (7693), 511-514.
49.Sandford, G., Elemental fluorine in organic chemistry (1997-2006). *J Fluorine Chem* **2007,** *128* (2), 90-104.
50.Taylor, S. D.; Kotoris, C. C.; Hum, G., Recent advances in electrophilic fluorination. *Tetrahedron* **1999,** *55* (43), 12431-12477.
51.Lal, G. S.; Pez, G. P.; Syvret, R. G., Electrophilic NF fluorinating agents. *Chemical Reviews* **1996,** *96* (5), 1737-1755.
52.Fier, P. S.; Hartwig, J. F., Selective C-H Fluorination of Pyridines and Diazines Inspired by a Classic Amination Reaction. *Science* **2013,** *342* (6161), 956-960.
53.Chan, K. S. L.; Wasa, M.; Wang, X. S.; Yu, J. Q., Palladium(II)-Catalyzed Selective Monofluorination of Benzoic Acids Using a Practical Auxiliary: A Weak-Coordination Approach. *Angew Chem Int Edit* **2011,** *50* (39), 9081-9084.
54.Hull, K. L.; Anani, W. Q.; Sanford, M. S., Palladium-catalyzed fluorination of carbon-hydrogen bonds. *J Am Chem Soc* **2006,** *128* (22), 7134-7135.
55.Huchet, Q. A.; Kuhn, B.; Wagner, B.; Kratochwil, N. A.; Fischer, H.; Kansy, M.; Zimmerli, D.; Carreira, E. M.; Muller, K., Fluorination Patterning: A Study of Structural Motifs That Impact Physicochemical Properties of Relevance to Drug Discovery. *Journal of Medicinal Chemistry* **2015,** *58* (22), 9041-9060.
56.Morgenthaler, M.; Schweizer, E.; Hoffmann-Roder, A.; Benini, F.; Martin, R. E.; Jaeschke, G.; Wagner, B.; Fischer, H.; Bendels, S.; Zimmerli, D.; Schneider, J.; Diederich, F.; Kansy, M.; Mueller, K., Predicting properties and tuning physicochemical in lead optimization: Amine basicities. *Chemmedchem* **2007,** *2* (8), 1100-1115.
57.Dawadi, S.; Viswanatham, K.; Boshoff, H. I.; Barry, C. E.; Aldrich, C. C., Investigation and Conformational Analysis of Fluorinated Nucleoside Antibiotics Targeting Siderophore Biosynthesis. *J Org Chem* **2015,** *80* (10), 4835-4850.
58.Neres, J.; Engelhart, C. A.; Drake, E. J.; Wilson, D. J.; Fu, P.; Boshoff, H. I.; Barry, C. E.; Gulick, A. M.; Aldrich, C. C., Non-Nucleoside Inhibitors of BasE, an Adenylating Enzyme in the Siderophore Biosynthetic Pathway of the Opportunistic Pathogen Acinetobacter baumannii. *Journal of Medicinal Chemistry* **2013,** *56* (6), 2385-2405.
59.Wang, J.; Sanchez-Rosello, M.; Acena, J. L.; del Pozo, C.; Sorochinsky, A. E.; Fustero, S.; Soloshonok, V. A.; Liu, H., Fluorine in Pharmaceutical Industry: Fluorine-Containing Drugs Introduced to the Market in the Last Decade (2001-2011). *Chemical Reviews* **2014,** *114* (4), 2432-2506.
60.Gallego, D.; Baquero, E. A., Recent Advances on Mechanistic Studies on C-H Activation Catalyzed by Base Metals. *Open Chem* **2018,** *16* (1), 1001-1058.
61.Ruiz-Castillo, P.; Buchwald, S. L., Applications of Palladium-Catalyzed C-N Cross-Coupling Reactions. *Chemical Reviews* **2016,** *116* (19), 12564-12649.
62.Cherney, A. H.; Kadunce, N. T.; Reisman, S. E., Enantioselective and Enantiospecific Transition-Metal-Catalyzed Cross-Coupling Reactions of Organometallic Reagents To Construct C-C Bonds. *Chemical Reviews* **2015,** *115* (17), 9587-9652.
63.Hartwig, J. F., Regioselectivity of the borylation of alkanes and arenes. *Chemical Society Reviews* **2011,** *40* (4), 1992-2002.
64.Cheng, C.; Hartwig, J. F., Catalytic Silylation of Unactivated C-H Bonds. *Chemical Reviews* **2015,** *115* (17), 8946-8975.
65.Dorel, R.; Echavarren, A. M., Gold(I)-Catalyzed Activation of Alkynes for the Construction of Molecular Complexity. *Chemical Reviews* **2015,** *115* (17), 9028-9072.
66.Souillart, L.; Cramer, N., Catalytic C-C Bond Activations via Oxidative Addition to Transition Metals. *Chemical Reviews* **2015,** *115* (17), 9410-9464.
67.Liu, W. P.; Ackermann, L., Manganese-Catalyzed C-H Activation. *Acs Catalysis* **2016,** *6* (6), 3743-3752.
68.Omer, H. M.; Liu, P., Computational Study of the Ni-Catalyzed C-H Oxidative Cycloaddition of Aromatic Amides with Alkynes. *Acs Omega* **2019,** *4* (3), 5209-5220.
69.Chink, P.; Morris, R., Getting Down to Earth: The Renaissance of Catalysis with Abundant Metals. *Accounts Chem Res* **2015,** *48* (9), 2495-2495.
70.Liu, J. D.; Chen, G. S.; Tan, Z., Copper-Catalyzed or -Mediated C-H Bond Functionalizations Assisted by Bidentate Directing Groups. *Adv Synth Catal* **2016,** *358* (8), 1174-1194.
71.Daugulis, O.; Roane, J.; Tran, L. D., Bidentate, Monoanionic Auxiliary-Directed Functionalization of Carbon-Hydrogen Bonds. *Accounts Chem Res* **2015,** *48* (4), 1053-1064.
72.Son, J., Sustainable manganese catalysis for late-stage C-H functionalization of bioactive structural motifs. *Beilstein J Org Chem* **2021,** *17*, 1733-1751.
73.Hu, Y. Y.; Zhou, B. W.; Wang, C. Y., Inert C-H Bond Transformations Enabled by Organometallic Manganese Catalysis. *Accounts Chem Res* **2018,** *51* (3), 816-827.
74.Aneeja, T.; Neetha, M.; Afsina, C. M. A.; Anilkumar, G., Recent advances and perspectives in manganese-catalyzed C-H activation. *Catal Sci Technol* **2021,** *11* (2), 444-458.
75.Trinh, C. H.; Hunter, T.; Stewart, E. E.; Phillips, S. E. V.; Hunter, G. J., Purification, crystallization and X-ray structures of the two manganese superoxide dismutases from Caenorhabditis elegans. *Acta Crystallogr F* **2008,** *64*, 1110-1114.
76.Liu, W.; Groves, J. T., Manganese Porphyrins Catalyze Selective C-H Bond Halogenations. *J Am Chem Soc* **2010,** *132* (37), 12847-12849.
77.Tarantino, G.; Hammond, C., Catalytic C(sp(3))-F bond formation: recent achievements and pertaining challenges. *Green Chem* **2020,** *22* (16), 5195-5209.
78.Liu, W.; Huang, X. Y.; Groves, J. T., Oxidative aliphatic C-H fluorination with manganese catalysts and fluoride ion. *Nat Protoc* **2013,** *8* (12), 2348-2354.
79.Li, G.; Dilger, A. K.; Cheng, P. T.; Ewing, W. R.; Groves, J. T., Selective C-H Halogenation with a Highly Fluorinated Manganese Porphyrin. *Angew Chem Int Edit* **2018,** *57* (5), 1251-1255.
80.Jin, N.; Ibrahim, M.; Spiro, T. G.; Groves, J. T., Trans-dioxo manganese(V) Porphyrins. *J Am Chem Soc* **2007,** *129* (41), 12416-+.
81.Liu, W.; Groves, J. T., Manganese Catalyzed C-H Halogenation. *Accounts Chem Res* **2015,** *48* (6), 1727-1735.

82.Du, X.; Zhang, H.; Lu, Y.; Wang, A. H.; Shi, P.; Li, Z. S., Fluorination reaction on an inactive sp(3) C-H bond mediated by manganese porphyrin catalysts: A theoretical study. *Comput Theor Chem* **2017,** *1115*, 330-334.
83.Hirao, H.; Kumar, D.; Que, L., Jr.; Shaik, S., Two-State Reactivity in Alkane Hydroxylation by Non-Heme Iron-Oxo Complexes. *J. Am. Chem. Soc.* **2006,** *128* (26), 8590-8606.
84.Shaik, S.; Danovich, D.; Fiedler, A.; Schroder, D.; Schwarz, H., 2-State Reactivity in Organometallic Gas-Phase Ion Chemistry. *Helv Chim Acta* **1995,** *78* (6), 1393-1407.
85.Schroder, D.; Shaik, S.; Schwarz, H., Two-state reactivity as a new concept in organometallic chemistry. *Acc. Chem. Res.* **2000,** *33* (3), 139-145.
86.Abram, S.-L.; Monte-Perez, I.; Pfaff, F. F.; Farquhar, E. R.; Ray, K., Evidence of Two-State Reactivity in Alkane Hydroxylation by Lewis-Acid Bound Copper-Nitrene Complexes. *Chemical Communications* **2014,** *50* (69), 9852-9854.
87.Rohde, J. U.; Que, L., Axial coordination of carboxylate activates the non-heme Fe-IV = O unit. *Angew Chem Int Edit* **2005,** *44* (15), 2255-2258.
88.Bukowski, M. R.; Koehntop, K. D.; Stubna, A.; Bominaar, E. L.; Halfen, J. A.; Munck, E.; Nam, W.; Que, L., A thiolate-ligated nonheme oxoiron(IV) complex relevant to cytochrome P450. *Science* **2005,** *310* (5750), 1000-1002.
89.Pestovsky, O.; Stoian, S.; Bominaar, E. L.; Shan, X. P.; Munck, E.; Que, L.; Bakac, A., Aqueous Fe-IV=O: Spectroscopic identification and oxo-group exchange. *Angew Chem Int Edit* **2005,** *44* (42), 6871-6874.
90.Decker, A.; Rohde, J. U.; Que, L.; Solomon, E. I., Spectroscopic and quantum chemical characterization of the electronic structure and bonding in a non-heme Fe-IV=O complex. *J Am Chem Soc* **2004,** *126* (17), 5378-5379.
91.Decker, A.; Solomon, E. I., Comparison of Fe-IV = O heme and non-heme species: Electronic structures, bonding, and reactivities. *Angew Chem Int Edit* **2005,** *44* (15), 2252-2255.
92.Schoneboom, J. C.; Neese, F.; Thiel, W., Toward identification of the Compound I reactive intermediate in cytochrome P450 chemistry: A QM/MM study of its EPR and Mossbauer parameters. *J Am Chem Soc* **2005,** *127* (16), 5840-5853.
93.Hohenberger, J.; Ray, K.; Meyer, K., The biology and chemistry of high-valent iron-oxo and iron-nitrido complexes. *Nat Commun* **2012,** *3*.
94.Price, J. C.; Barr, E. W.; Glass, T. E.; Krebs, C.; Bollinger, J. M., Evidence for hydrogen abstraction from C1 of taurine by the high-spin Fe(IV) intermediate detected during oxygen activation by taurine :alpha-ketoglutarate dioxygenase (TauD). *J Am Chem Soc* **2003,** *125* (43), 13008-13009.
95.Price, J. C.; Barr, E. W.; Tirupati, B.; Bollinger, J. M.; Krebs, C., The first direct characterization of a high-valent iron intermediate in the reaction of an alpha-ketoglutarate-dependent dioxygenase: A high-spin Fe(IV) complex in taurine/alpha-ketoglutarate dioxygenase (TauD) from Escherichia coli (vol 42, pg 7497, 2003). *Biochemistry-Us* **2004,** *43* (4), 1134-1134.
96.Fujimori, D. G.; Barr, E. W.; Matthews, M. L.; Koch, G. M.; Yonce, J. R.; Walsh, C. T.; Bollinger, J. M.; Krebs, C.; Riggs-Gelasco, P. J., Spectroscopic evidence for a high-spin Br-Fe(IV)-Oxo intermediate in the alpha-ketoglutarate-dependent halogenase CytC3 from Streptomyces. *J Am Chem Soc* **2007,** *129* (44), 13408-+.
97.Mehmood, R.; Vennelakanti, V.; Kulik, H. J., Spectroscopically Guided Simulations Reveal Distinct Strategies for Positioning Substrates to Achieve Selectivity in Nonheme Fe(II)/alpha-Ketoglutarate-Dependent Halogenases. *Acs Catal* **2021,** *11* (19), 12394-12408.
98.Song, W. J.; Seo, M. S.; George, S. D.; Ohta, T.; Song, R.; Kang, M. J.; Tosha, T.; Kitagawa, T.; Solomon, E. I.; Nam, W., Synthesis, characterization, and reactivities of manganese(V)-oxo porphyrin complexes. *J Am Chem Soc* **2007,** *129* (5), 1268-1277.
99.Zhang, R.; Newcomb, M., Laser flash photolysis formation and direct kinetic studies of manganese(V)-oxo porphyrin intermediates. *J Am Chem Soc* **2003,** *125* (41), 12418-12419.
100.Jin, N.; Groves, J. T., Unusual kinetic stability of a ground-state singlet oxomanganese(V) porphyrin. Evidence for a spin state crossing effect. *J Am Chem Soc* **1999,** *121* (12), 2923-2924.
101.Groves, J. T.; Lee, J. B.; Marla, S. S., Detection and characterization of an oxomanganese(V) porphyrin complex by rapid-mixing stopped-flow spectrophotometry. *J Am Chem Soc* **1997,** *119* (27), 6269-6273.
102.Hull, J. F.; Balcells, D.; Sauer, E. L. O.; Raynaud, C.; Brudvig, G. W.; Crabtree, R. H.; Eisenstein, O., Manganese Catalysts for C-H Activation: An Experimental/Theoretical Study Identifies the Stereoelectronic Factor That Controls the Switch between Hydroxylation and Desaturation Pathways. *J Am Chem Soc* **2010,** *132* (22), 7605-7616.
103.Yerien, D. E.; Bonesi, S.; Postigo, A., Fluorination methods in drug discovery. *Org Biomol Chem* **2016,** *14* (36), 8398-8427.
104.Hanwell, M. D.; Curtis, D. E.; Lonie, D. C.; Vandermeersch, T.; Zurek, E.; Hutchison, G. R., Avogadro: an advanced semantic chemical editor, visualization, and analysis platform. *J Cheminformatics* **2012,** *4*.
105.Rappe, A. K.; Casewit, C. J.; Colwell, K. S.; Goddard, W. A.; Skiff, W. M., Uff, a Full Periodic-Table Force-Field for Molecular Mechanics and Molecular-Dynamics Simulations. *J Am Chem Soc* **1992,** *114* (25), 10024-10035.
106.Ufimtsev, I. S.; Martinez, T. J., Quantum Chemistry on Graphical Processing Units. 3. Analytical Energy Gradients, Geometry Optimization, and First Principles Molecular Dynamics. *J Chem Theory Comput* **2009,** *5* (10), 2619-2628.
107.Lee, C. T.; Yang, W. T.; Parr, R. G., Development of the Colle-Salvetti Correlation-Energy Formula into a Functional of the Electron-Density. *Phys Rev B* **1988,** *37* (2), 785-789.
108.Becke, A. D., Density-Functional Thermochemistry .3. The Role of Exact Exchange. *J Chem Phys* **1993,** *98* (7), 5648-5652.
109.Stephens, P. J.; Devlin, F. J.; Chabalowski, C. F.; Frisch, M. J., Ab-Initio Calculation of Vibrational Absorption and Circular-Dichroism Spectra Using Density-Functional Force-Fields. *J Phys Chem-Us* **1994,** *98* (45), 11623-11627.
110.Grimme, S.; Antony, J.; Ehrlich, S.; Krieg, H., A consistent and accurate ab initio parametrization of density functional dispersion correction (DFT-D) for the 94 elements H-Pu. *J Chem Phys* **2010,** *132* (15).
111.Grimme, S.; Ehrlich, S.; Goerigk, L., Effect of the Damping Function in Dispersion Corrected Density Functional Theory. *J Comput Chem* **2011,** *32* (7), 1456-1465.
112.Hay, P. J.; Wadt, W. R., Abinitio Effective Core Potentials for Molecular Calculations - Potentials for the Transition-Metal Atoms Sc to Hg. *J Chem Phys* **1985,** *82* (1), 270-283.

113.Wadt, W. R.; Hay, P. J., Abinitio Effective Core Potentials for Molecular Calculations - Potentials for Main Group Elements Na to Bi. *J Chem Phys* **1985,** *82* (1), 284-298.
114.Ditchfield, R.; Hehre, W. J.; Pople, J. A., Self-Consistent Molecular-Orbital Methods .9. Extended Gaussian-Type Basis for Molecular-Orbital Studies of Organic Molecules. *J Chem Phys* **1971,** *54* (2), 724-+.
115.Kastner, J.; Carr, J. M.; Keal, T. W.; Thiel, W.; Wander, A.; Sherwood, P., DL-FIND: An Open-Source Geometry Optimizer for Atomistic Simulations. *J Phys Chem A* **2009,** *113* (43), 11856-11865.
116.Saunders, V. R.; Hillier, I. H., Level-Shifting Method for Converging Closed Shell Hartree-Fock Wave-Functions. *Int J Quantum Chem* **1973,** *7* (4), 699-705.
117.Lange, A. W.; Herbert, J. M., A smooth, nonsingular, and faithful discretization scheme for polarizable continuum models: The switching/Gaussian approach. *J Chem Phys* **2010,** *133* (24).
118.York, D. M.; Karplus, M., A smooth solvation potential based on the conductor-like screening model. *J Phys Chem A* **1999,** *103* (50), 11060-11079.
119.Liu, F.; Luehr, N.; Kulik, H. J.; Martinez, T. J., Quantum Chemistry for Solvated Molecules on Graphical Processing Units Using Polarizable Continuum Models. *J Chem Theory Comput* **2015,** *11* (7), 3131-3144.
120.Bondi, A., Van Der Waals Volumes + Radii. *J Phys Chem-Us* **1964,** *68* (3), 441-+.
121.Janet, J. P.; Ramesh, S.; Duan, C.; Kulik, H. J., Accurate Multiobjective Design in a Space of Millions of Transition Metal Complexes with Neural-Network-Driven Efficient Global Optimization. *Acs Central Sci* **2020,** *6* (4), 513-524.
122.Batsanov, S. S., Van der Waals radii of elements. *Inorganic Materials* **2001,** *37* (9), 871– 885.
123.Ioannidis, E. I.; Kulik, H. J., Towards quantifying the role of exact exchange in predictions of transition metal complex properties. *J Chem Phys* **2015,** *143* (3).
124.Janet, J. P.; Kulik, H. J., Predicting electronic structure properties of transition metal complexes with neural networks. *Chem Sci* **2017,** *8* (7), 5137-5152.
125.Ioannidis, E. I.; Gani, T. Z. H.; Kulik, H. J., molSimplify: A toolkit for automating discovery in inorganic chemistry. *J Comput Chem* **2016,** *37* (22), 2106-2117.
126.O'Boyle, N. M.; Banck, M.; James, C. A.; Morley, C.; Vandermeersch, T.; Hutchison, G. R., Open Babel: An open chemical toolbox. *J Cheminformatics* **2011,** *3*.
127.O'Boyle, N. M.; Morley, C.; Hutchison, G. R., Pybel: a Python wrapper for the OpenBabel cheminformatics toolkit. *Chem Cent J* **2008,** *2*.